New proxies for second-order cumulants of conserved charges in heavy-ion collisions within the EPOS4 framework

Johannes Jahan [1,2,*] Claudia Ratti [1] Maria Stefaniak [3,4] and Klaus Werner [2]

[1] *Department of Physics - University of Houston, Houston, Texas 77204, USA*

[2] *SUBATECH, University of Nantes - IN2P3/CNRS - IMT Atlantique, 44300 Nantes, France*

[3] *Department of Physics - The Ohio State University, Columbus, Ohio 43210, USA*

[4] *GSI Helmholtz Centre for Heavy Ion Research, 64291 Darmstadt, Germany*

(Received 7 June 2024; accepted 14 August 2024; published 11 September 2024)

Proxies for cumulants of baryon number B, electric charge Q, and strangeness S are usually measured in heavy-ion collisions via moments of net-number distribution of given hadronic species. Since these cumulants of conserved charges are expected to be sensitive to the existence of a critical point in the phase diagram of nuclear matter, it is crucial to ensure that the proxies used as substitutes are as close to them as possible. Hence, we use the EPOS4 framework to generate Au + Au collisions at several collision energies of the BNL Relativistic Heavy Ion Collider beam energy scan. We compute second-order net cumulants of π, K, and p, for which experimental data have been published as well as the corresponding conserved charge cumulants. We then compare them with proxies, defined in previous lattice QCD and hadron resonance gas model studies, which are shown to reproduce more accurately their associated conserved charge cumulants. We investigate the impact of hadronic rescatterings occurring in the late evolution of the system on these quantities, as well as the amount of signal actually originating from the bulk medium which endures a phase transition.

DOI: 10.1103/PhysRevC.110.035201

I. INTRODUCTION

For several decades now, heavy-ion collisions (HICs) at relativistic energies have been used to study the properties of nuclear matter, and to map the phase diagram of quantum chromodynamics (QCD). Since the creation of a deconfined state of quarks and gluons at very high temperature, the quark-gluon plasma (QGP) has been brought to light by several experiments at the BNL Relativistic Heavy Ion Collider (RHIC) [1–4], understanding the nature of the transition from a hadronic phase to the QGP has been one of the main focuses in the field. On the theoretical side, first-principle calculations from lattice QCD simulations predict a crossover at low baryon chemical potential μ_B [5–7], which seems confirmed by experimental results from RHIC and the CERN Large Hadron Collider (LHC) [8]. Several approaches predict a first-order phase transition at high μ_B, which would imply the existence of a critical point on the QCD phase diagram [9–12]. The RHIC beam energy scan (BES) program has thus been set up to scan a large region of the phase diagram at finite μ_B, by colliding $^{197}_{79}$Au nuclei in a wide range of center-of-mass energies. They have collected data at collision energies from $\sqrt{s_{NN}} = 200$ GeV down to 7.7 GeV in collider mode through phases I and II [13,14], and even down to $\sqrt{s_{NN}} = 3.0$ GeV through the fixed-target program [15]. Indeed, one of the main goals of this program is to search for the existence of a first-order phase transition, and thus to assess the location of the hypothetical critical point.

To probe the existence of a critical point in the QCD phase diagram, susceptibilities of conserved charges such as baryon number B, electric charge Q, and strangeness S are the theoretical quantities of choice because they diverge in the vicinity of the critical point. They can be calculated as derivatives of the pressure p with respect to the chemical potential of the corresponding conserved charge [16]:

$$\chi^{BQS}_{ijk} = \frac{\partial^{i+j+k}(p/T^4)}{(\partial\hat{\mu}_B)^i(\partial\hat{\mu}_Q)^j(\partial\hat{\mu}_S)^k}\,, \tag{1}$$

where $\hat{\mu}_i = \mu_i/T$. Because the pressure is directly related to the partition function, they quantify how much the latter is modified under variations of the different chemical potentials and are thus sensitive to radical changes in the state of nuclear matter, e.g., the effect of a first-order phase transition or a critical point. One can also relate the susceptibilities to net cumulants of conserved charges. For the case of second-order cumulants, which will be at the center of our study, these relationships are

$$\chi^{XY}_{11} = \frac{\langle N_X N_Y\rangle - \langle N_X\rangle\langle N_Y\rangle}{VT^3} = \frac{\sigma^{XY}_{11}}{VT^3}, \tag{2}$$

$$\chi^{X}_{2} = \frac{\langle {N_X}^2\rangle - \langle N_X\rangle^2}{VT^3} = \frac{\sigma^{2}_{X}}{VT^3}, \tag{3}$$

*Contact author: jahan.johannes@gmail.com

where σ_2^X and σ_{11}^{XY} are respectively the variance and covariance of the net numbers of conserved charges, N_X or N_Y [17]. In the context of HICs, the (co)variances of net-hadron multiplicities can be used as probes for conserved charges [18]. So far, because they are the most abundant and easiest species to identify in experiments, net-proton cumulants have been used as proxies for B fluctuations [19], net-kaon cumulants have been used as proxies for S fluctuations [20], and net-multiplicity cumulants of combined identified hadrons have been used as proxies for Q fluctuations [21]. By convention, the net numbers N_b of any baryon species b are defined as the difference between number of baryons and number of antibaryons, $n_b - n_{\bar{b}}$, while for meson species m the net number N_m is usually defined as the difference between positively charged mesons and negatively charged ones, $n_{m^+} - n_{m^-}$.

However, using HICs to probe the phase diagram of nuclear matter comes with a lot of limitations. While on the theoretical side, most predictions are obtained from grand-canonical ensemble calculations, assuming thermal equilibrium and infinite volume, the system created in heavy-ion collisions is very short-lived, finite, small-sized, and experiences rapid expansion [22]. Moreover, the volume and temperature are not accessible through measurements, and are changing during the evolution of a single event. It has been thus proposed to use ratios of net cumulants to compare with theoretical predictions of susceptibilities in order to get rid of the volume and temperature dependence at leading order [23]. Finally, using particles as experimental probes shows severe limitations, first of all because not all hadrons can be experimentally detected. For example, neutral hadrons can carry, e.g., baryon number or strangeness (like neutrons and Λ baryons). Besides, measuring conserved charges through hadron distributions includes additional fluctuations, since particle production is a quantum process, thus probabilistic in essence.

It is hence important to find hadronic proxies that reflect conserved charge fluctuations as accurately as possible through the cumulants of their net-multiplicity distributions. In this paper, we want to address this question for second-order cumulants of conserved charges, by comparing proxies measured by the STAR Collaboration in Ref. [21] against new proxies inspired by Ref. [24] and with their corresponding conserved charge quantities, measured in Au + Au simulations in the RHIC beam energy range. We employ the EPOS4 event generator [25] and take advantage of its modular design to compare the several observables of interests as measured through the final-state particle distribution with the same quantities at hadronization time, to quantify the impact of the hadronic rescatterings on them. Finally, because EPOS4 relies on a separate treatment of the bulk matter and high-p_T particles to model the presence of a fluid in the system, as an imitation of the QGP, we check how much of the signal of these cumulant proxies actually originates from the deconfined medium.

In Sec. II, we start by describing the different observables we use in our work, before introducing EPOS4 in Sec. III, the event generator used to produce the simulations of Au + Au collisions on which relies our study. Then, after having discussed the details of our analysis and the simulations in Sec. IV, we present our results and their interpretation them in Sec. V, and then finally summarize the conclusions of our study and mention potential outlooks in Sec. VI.

II. PROXIES OF CONSERVED CHARGE CUMULANTS

As mentioned in Sec. I, one way to probe fluctuations of conserved charges in HICs is to measure fluctuations in the net-distribution of hadronic species used as proxies. However, choosing appropriate proxies is essential to ensure that the observables we study reflect properly the corresponding conserved charge fluctuations. This is the motivation of our study. In this section, we present the commonly used experimental proxies at first, before introducing the ones we propose because of their more accurate description of conserved charges in the context of HICs. Our proposed proxies, taken in part from a previous work [24], will then be tested against those commonly measured in experiment, as well as the corresponding cumulants of conserved charges, through realistic simulations of HICs collisions generated with EPOS4.

A. STAR proxies

The experimental results on which this study is based are second-order diagonal and off-diagonal cumulants (also referred to as variances and covariances) from net-π, net-K, and net-p distributions published by the STAR Collaboration in Ref. [21]. They present, for Au + Au collisions at $\sqrt{s_{NN}} =$ 7.7, 11.5, 14.5, 19.6, 27, 39, 62.4, and 200 GeV, the different (co)variances:.

$$\begin{pmatrix} \sigma_\pi^2 & \sigma_{\pi p}^{11} & \sigma_{\pi K}^{11} \\ \sigma_{\pi pK}^{11} & \sigma_p^2 & \sigma_{pK}^{11} \\ \sigma_{\pi K}^{11} & \sigma_{pK}^{11} & \sigma_K^2 \end{pmatrix}, \tag{4}$$

within a pseudorapidity window $|\eta| < 0.5$ and for particles with $0.4 < p_T < 1.6$ GeV. Results are notably shown as a function of the centrality class for 0%–80% centrality (through the mean number of participant nucleons $\langle N_{\text{part}} \rangle$) for each collision energy, corrected for centrality bin-width effect (CBWE) [26]. These (co)variances are then used to build proxy ratios for net-charge cumulant ratios in order to get rid of the explicit dependence on T and V, which are not experimentally accessible event-by-event. The proxy ratios defined by STAR are the following (in parentheses we indicate the corresponding ratio of conserved charge fluctuations they are meant to represent):

$$C_{Qp} = \frac{\sigma_{Qp}^{11}}{\sigma_p^2} \left(\simeq \frac{\chi_{11}^{QB}}{\chi_2^B} \right), \quad C_{QK} = \frac{\sigma_{QK}^{11}}{\sigma_K^2} \left(\simeq \frac{\chi_{11}^{QS}}{\chi_2^S} \right),$$
$$C_{pK} = \frac{\sigma_{pK}^{11}}{\sigma_K^2} \left(\simeq \frac{\chi_{11}^{BS}}{\chi_2^S} \right), \tag{5}$$

where the covariance of Q with any species h is related to the covariances displayed in the matrix of Eq. (4) through $\sigma_{Qh}^{11} = \sigma_{\pi h}^{11} + \sigma_{Kh}^{11} + \sigma_{ph}^{11}$. These proxy ratios are displayed as

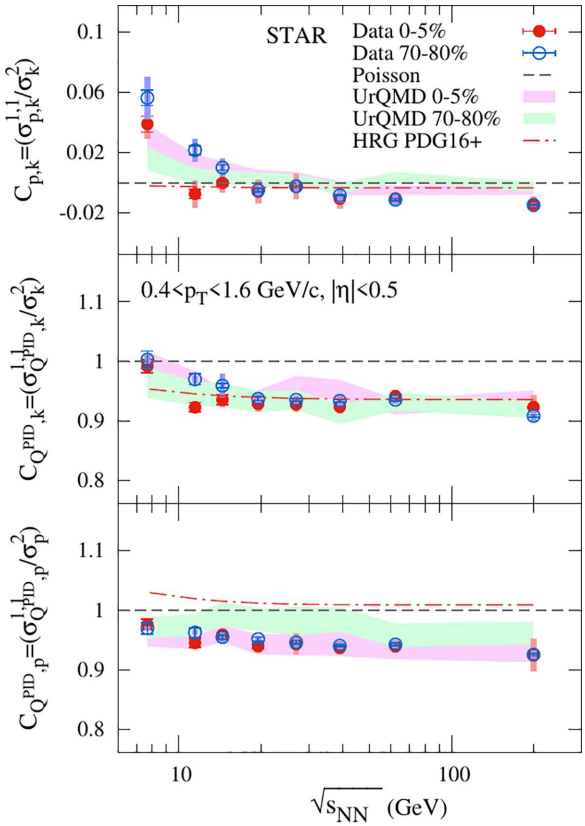

FIG. 1. Energy dependence of the cumulants ratios C_{pK}, C_{QK} for central (0%–5%) and peripheral (70%–80%) Au-Au collisions within $|\eta| < 0.5$ and $0.4 < p_T < 1.6$ GeV. Results from STAR have systematic errors indicated by the boxes and statistical ones by bars. Poisson baseline, UrQMD simulations results, and calculations using the HRG model including the PDG16+ [29] particles set are displayed for comparison [21].

functions of $\langle N_{\text{part}} \rangle$ too, but also as functions of collision energy for most central (0%–5%) and most peripheral (70%–80%) collisions. These last results are of particular importance as they are expected to hint at the existence of the critical point, since decreasing the collision energy increases the baryonic chemical potential of the system created in the collision. Note that any proxy involving Q is calculated through measured net numbers of identified charged π, K, and $p/\overline{p}$, and not directly from unidentified charged particle tracks. This is done to ensure a proper estimation of detection efficiency correction, as pointed out in Refs. [27,28].

One interesting observation from the results shown in Fig. 1 is the change of sign of the C_{pK} ratio. While it shows no centrality dependence for $\sqrt{s_{NN}} \geqslant 19.6$ GeV, it changes sign at lower collision energies, where it also starts to show a centrality dependence. According to Ref. [23], this could be due to a modification of the dynamics in the system, hinting for a change in the phase from which the studied correlations arise. This motivates even more the need to provide accurate proxies for conserved charge fluctuations, as this change of dynamics has also been shown through the observed disappearance of partonic collectivity in Au + Au collisions at $\sqrt{s_{NN}} = 3$ GeV [30].

In this paper, we systematically compare our results with the data from Ref. [21], primarily as a benchmark to see if EPOS4 simulations are able to reproduce experimental results of net-multiplicity (co)variances for light hadrons. This will complement all the results from EPOS4 published so far, in particular those on particle production and flow for BES energies in Refs. [31,32]. Moreover, it is also interesting to compare those data with EPOS4 simulations and look for any significant deviation, because the latter can be considered as another noncritical baseline, as will be explained in Sec. III.

B. New improved proxies

The work presented here has also been motivated by a theoretical study of proxies for fluctuations of B, Q, and S [24]. In this paper, the HRG model has been used to quantify how much every different hadronic species experimentally measured contributes to the lattice QCD susceptibilities in the region where both approaches overlap. As HRG relies on a description of QCD matter in terms of a gas of noninteracting hadrons and resonances, it is by construction quite straightforward to express susceptibilities in terms of a sum of hadronic contributions:

$$\chi^{BQS}_{ijk}(T,\vec{\hat{\mu}}) = \sum_R \sum_{h\in\text{stable}} (P_{R\to h})^l (B_h)^i (Q_h)^j (S_h)^k \times \frac{\partial^l p_h/T^4}{(\partial\hat{\mu}_B)^i (\partial\hat{\mu}_Q)^j (\partial\hat{\mu}_S)^k}. \tag{6}$$

In this equation, $l = i + j + k$ (with $l = 2$ for our study). The R index refers to resonances and h to the stable hadrons these resonances can decay into, with $P_{R\to h}$ representing the branching ratio for R decaying into h. B_h, Q_h, and S_h are the respective baryon number, electric charge, and strangeness of hadron species h, and p_h is the pressure due to hadron species h. Thanks to the statistical nature of the HRG model, one can easily integrate the particle distributions over only a fraction of the complete phase space in order to reproduce the finite coverage of detectors in experiments.

By doing so, the authors of Ref. [24] have been able to construct new proxies based on the variance of net distributions of some hadron species, that have been shown to reproduce susceptibility ratios very accurately. Note, however, that they have not considered the contribution originating from the probabilistic nature of hadron decays in the variances used as proxies, which effect have been highlighted, for instance, in Refs. [33,34]. Some of the proxy ratios, denoted here as $\tilde{C}_{QS}$ and $\tilde{C}_{BS}$ ($\tilde{C}'_{BS}$) and respectively probing the same quantities as the STAR proxies C_{QK} and C_{pK} from Eq. (5), are defined as

$$\tilde{C}_{QS} = \frac{1}{2}\frac{\sigma_K^2}{\sigma_K^2+\sigma_\Lambda^2}\left(\cong\frac{\chi_{11}^{QS}}{\chi_2^S}\right), \tag{7}$$

$$\tilde{C}_{BS} = \frac{\sigma_\Lambda^2}{\sigma_K^2+\sigma_\Lambda^2}, \tag{8}$$

$$\tilde{C}'_{BS} = \frac{\sigma_\Lambda^2+2\sigma_\Xi^2+3\sigma_\Omega^2}{\sigma_\Lambda^2+4\sigma_\Xi^2+9\sigma_\Omega^2+\sigma_K^2}\left(\cong\frac{-\chi_{11}^{BS}}{\chi_2^S}\right). \tag{9}$$

One can observe that these proxy ratios are only based on single hadron species variances, and do not involve any

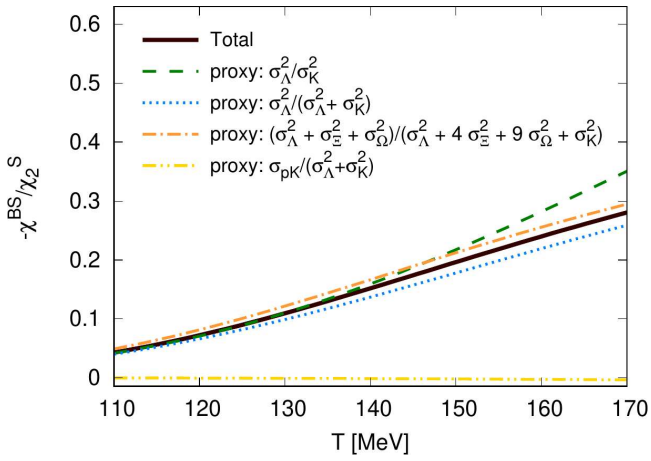

FIG. 2. Comparison of several proxy ratios for BS correlations obtained via HRG model calculations, plotted as a function of T. As a reference, the related ratio of exact susceptibilities calculated with lattice QCD (marked as "Total") is displayed [24].

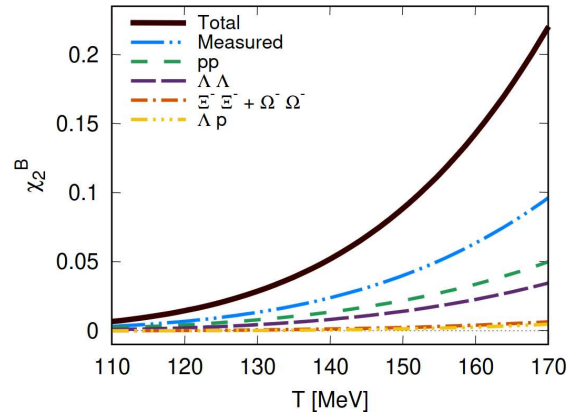

FIG. 3. Breakdown of the different final-state hadronic contributions to the diagonal correlators of χ_2^B. The total contribution and the measured part are shown as solid black and dashed-dotted blue lines, respectively. The main single contributions from measured hadronic observables are shown with different colored dashed and dashed-dotted lines [24].

covariance between different species. This is because cross-correlators between different conserved charges, χ_{11}^{XY}, receive most of their contribution from the variances $\sigma_{h_1}^2$ of single species h_1 carrying both charges X and Y. Only a very small fraction of χ_{11}^{XY} actually comes from covariances $\sigma_{h_1h_2}$ between two different species h_1 and h_2, each of them carrying one of the two conserved charges X and Y. Note also that two ratios, $\tilde{C}_{BS}$ and $\tilde{C}'_{BS}$, have been proposed as proxies for χ_{11}^{BS}/χ_2^S. Both of them are built in the same way, $\tilde{C}'_{BS}$ being an extension of $\tilde{C}_{BS}$ that includes in addition the contribution of multistrange baryons. Even though this extra contribution in $\tilde{C}'_{BS}$ (represented by the dashed-dotted orange line on Fig. 2) does not improve significantly the situation compared with $\tilde{C}_{BS}$ (shown by the dotted blue line), we still compute both of them to see how they compare in event generator simulations.

However, no proxy for χ_{11}^{QB}/χ_2^B has been proposed in Ref. [24], because authors claim that isospin randomization of the nucleons, due to reactions of the type [35,36]

$$p + \pi^{0/-} \leftrightarrow \Delta^{+/0} \leftrightarrow n + \pi^{+/0}$$

happening in the hadronic phase to both baryons and antibaryons, and occurring for several cycles, prevents from building a good proxy for this ratio. Since STAR measured this quantity through the proxy C_{Qp}, introduced in Eq. (5), we still want to propose here a new proxy. We start with the numerator $\chi_{11}^{QB}(=\chi_{11}^{BQ})$, which cannot be probed by σ_p^2 alone since it is affected by isospin randomization, but instead by $\sigma_{p\pi} + \sigma_p^2$, which is not. The use of this quantity was already attempted in Ref. [24], when trying to construct a proxy ratio for χ_{11}^{QB}/χ_2^Q. Next, we need a proxy for the denominator χ_2^B. Because isospin randomization leads to equilibrate the amount of protons and neutrons in the system, one can probe the nucleon variance using the proton one through $\sigma^2_{\text{Net-}N} = 2\sigma_p^2$ [24]. We propose to use the net-Λ variance in addition because it is the second major contributor to χ_2^B, as shown in Fig. 3. It is also used in the other proxy ratios (7), (8), and (9) and was already measured experimentally [37]. Therefore, we propose the proxy ratio

$$\tilde{C}_{QB} = \frac{\sigma_{\pi p}^{11} + \sigma_p^2}{2\sigma_p^2 + \sigma_\Lambda^2} \left(\cong \frac{\chi_{11}^{QB}}{\chi_2^B} \right), \tag{10}$$

to probe a similar quantity as the STAR proxy C_{Qp} from Eq. (5).

III. EPOS4

Event generators are essential simulation tools in modern high-energy physics phenomenology based on theoretical frameworks and enable bridging the gap between the fundamental theory (QCD) and experiments [38]. In this study, we employ EPOS4.0.0 [25], the latest version of the multipurpose event generator, released publicly through a dedicated web page [39]. EPOS4 is built to offer a realistic description of high-energy hadronic collisions from several GeV to several TeV per-nucleon center-of-mass energy. Testing the proxies for conserved charge fluctuations introduced in Sec. II aims thus at validating the study using lattice QCD data and HRG simulations on which these proxies are based. In addition, achieving this study through realistic simulations of HICs with EPOS4 offers a more direct connection with the experimental scenario and a meaningful comparison with experimental proxies already in use to probe fluctuations.

In EPOS4, the primary interactions are modeled through a multiple-interaction approach based on the S-matrix theory, including perturbative QCD calculations and saturation effects [40]. In EPOS4, major improvements have been achieved by ensuring a consistent treatment of saturation and factorization, through the implementation of a dynamical saturation scale within this energy-conserving parallel scattering framework [25,32]. The treatment of perturbative calculations has also been updated, with a particular care for heavy flavors [41].

The prehadrons formed through primary scatterings and remnants excitation are then split into two categories,

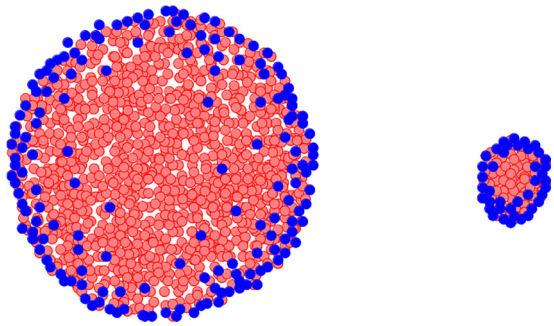

FIG. 4. Sketch of the core-corona separation for a "big" and a "small" system. The dots are prehadrons in the transverse plane, with red referring to prehadrons from the core, blue to prehadrons from the corona [44].

following a so-called "core-corona" procedure, as shown in Fig. 4, based on their density and some energy-loss considerations [42,43]. This procedure, applied at an initial time $\tau_0 = 1.5$ fm/c for HICs [31], has been discussed with many details in the context of EPOS4 in Ref. [44]. The hot and dense bulk matter made from low transverse momentum prehadrons, the "core," evolves following $(3+1)$-dimensional [$(3+1)$D] viscous hydrodynamics equations using VHLLE [45] and employing a simple crossover equation of state (EoS) matched with lattice QCD data [43]. Once the system has expanded and cooled down, it will hadronize when reaching an energy density $\epsilon_H = 0.57$ GeV/fm^3, based on a microcanonical procedure [44]. This is particularly important for simulating small systems, where few particles are produced, and hence local energy and charge conservation play an important role. On the other hand, prehadrons with high p_T (sufficient to escape the core) form the "corona," and may then still re-interact with the core hadrons through hadronic scatterings.

Hadronic rescatterings between all formed hadrons (also referred to as hadronic cascades) are simulated using UrQMD as an afterburner [46,47]. It models elastic scatterings, string and resonance excitations as well as $2 \to n$ processes and strangeness exchange reactions based on measured reaction cross sections, and includes 60 baryonic species plus 40 mesonic states.

For the work presented here, we take advantage of the modular construction of EPOS4, since one can access the distribution of particles at hadronization, just before hadrons are fed into UrQMD. This allows us to study the impact of hadronic cascades on fluctuation observables by comparing this distribution with the final-state particle one. Moreover, the core-corona procedure applied in EPOS4 allows us to differentiate particles originating from the bulk matter (the core in the EPOS4 framework) and those originating from hard processes (corona hadrons). Hence, one can extract the proportion of the total fluctuation signal measured in the final state that is actually coming from the core, which contains the potential critical fluctuations.

We want to mention that, among the improvements brought to the EPOS framework in EPOS4, it is now possible to use an EoS including a first-order phase transition and a critical point from the three-dimensional (3D) Ising-model universality class, such as, e.g., the one published by the BEST Collaboration [48] and its recent improvement [49] to model the hydrodynamical evolution of the core [50]. However, we do not use it for the HIC simulations used in this work, but employ a simple crossover EoS as mentioned previously. The main reason is that our goal is to compare different proxy observables with their corresponding conserved charge quantities, and to study the impact of hadronic cascades on them. We do not aim at investigating the effect of criticality on these observables, since EPOS4 does not propose the adequate framework for such investigation. In fact, it employs an "ordinary" hydrodynamical code that does not incorporate any out-of-equilibrium fluctuations nor charge dissipation relations, which are necessary to study the impact of critical behavior on the evolution of the system created in HICs. Several works are currently ongoing towards the development of hydrodynamics framework that would properly take fluctuations into account [51,52], which might eventually be included in EPOS4 in the future. Until then, EPOS4 can be considered as a noncritical baseline, especially when run with the crossover EoS employed here.

TABLE I. Total number of individual Au + Au events per collision energy simulated with EPOS4.

$\sqrt{s_{NN}}$	19.6 GeV	27 GeV	39 GeV	62.4 GeV	200 GeV
N_{evts}	2.5×10^6	2.5×10^6	2.5×10^6	2.0×10^6	1.5×10^6

IV. ANALYSIS DETAILS

For all the results presented in Sec. V, particle distributions have been evaluated using the same cuts employed by STAR in Ref. [21] to allow a direct comparison with their data. We take into account all particle distributions within a pseudorapidity window $|\eta| < 0.5$ and for particles with $0.4 < p_T < 1.6$ GeV. To correct from feed-down, we chose to consider only particles that have a vertex of origin located at less than 1 cm from the interaction vertex, instead of explicitly neglecting all secondary particles as EPOS4 would allow. This is to stay as close to the experimental analysis as possible, where they correct from contamination of secondary particles by considering only tracks with a distance of closest approach (DCA) to the primary vertex <1 cm.

In Table I, one can find the number of events simulated with EPOS4 for each of the collision energies shown in this work. Note that we only show EPOS4 results from $\sqrt{s_{NN}}$=19.6 GeV and above, although STAR data are available down to $\sqrt{s_{NN}} =$ 7.7 GeV. We choose to do so since a previous study of EPOS4 results, in the energy range of the BES, showed that the model is not applicable anymore below such collision energy [31]. In fact, a systematic study of p_T spectra of many light and strange hadrons at several collision energies has shown that EPOS4 fails at reproducing, even qualitatively, the available experimental data below $\sqrt{s_{NN}} = 19.6$ GeV. This is expected due to current limitations inherent to the approach employed to model the primary interactions. Thus, we only discuss here results in a collision energy range which is physically relevant to the model. All events used in this study have been

generated using the core-corona separation procedure, the so-called x3FF crossover equation of state mentioned in Sec. III with the VHLLE hydrodynamic model for the evolution of bulk matter and neglecting any jet-fluid interaction.

Another important aspect when studying cumulants of net-multiplicity distributions in HICs, is the definition of centrality classes, and how we correct cumulants from the CBWE [26]. For all results shown as functions of the number of participating nucleons $N_{\rm part}$, we compute (co)variances directly as functions of this observable, since it is accessible through our simulations. However, we do not use the actual $N_{\rm part}$ value from EPOS4 primary interaction model, but the Glauber estimated value based on the impact parameter. This way, we ensure the closest apple-to-apple comparison with the $N_{\rm part}$ values estimated for each centrality class in the STAR analysis [21]. For these results, we divide our distributions into 20 bins of width $\Delta N_{\rm part} = 20$, which broadly correspond to centrality classes of ≈5%. The advantage is that, using directly $N_{\rm part}$ to determine centrality, with such narrow bins in particular, reduces the volume fluctuations within a given centrality class compared with experimental centrality classes based on charged multiplicity. Moreover, a study of the CBWE has shown that second-order cumulants should not be affected much by this effect, for centrality classes smaller than 10% [26]. We have successfully tested this in EPOS4 simulations for collisions at $\sqrt{s_{NN}} = 200$ GeV, as shown in Appendix B of Ref. [53]. All results displayed as functions of collision energy $\sqrt{s_{NN}}$ for different centrality classes are obtained using the same centrality determination procedure.

The main goal of our study being to test the accuracy of the net-charge proxy cumulants introduced in Sec. II, we compare them with the actual net-B, net-Q, and net-S cumulants, which are computable from EPOS4 simulations because all particles are accessible. To make a relevant comparison with the proxy cumulants, we calculate the net-charge cumulants by considering the charges carried by all particles in the same phase space as the one used for the proxies and the STAR analysis, i.e., within a pseudorapidity window $|\eta| < 0.5$ and for particles with $0.4 < p_T < 1.6$ GeV. We apply the same DCA <1 cm criterion to select particles in order to correct from feed-down contamination and consider particles before weak decays, since the latter violates S conservation. Technical details about the way we perform the calculation of net-charge cumulants in the EPOS4 simulated events are provided in Appendix C of Ref. [53].

V. RESULTS AND DISCUSSION

In this section, we discuss the results of our study of the proxies for second-order cumulants of conserved charges, obtained through the analyses described in Sec. IV. We first show the (co)variances of different identified hadron species at several collision energies $\sqrt{s_{NN}}$, as functions of $N_{\rm part}$, for final-state particle distributions and also particle distributions just after hadronization, compared with experimental data from STAR [21]. From there, we build the different proxy ratios and compare them with their corresponding conserved charge cumulant ratios as well as with STAR data, still as functions of $N_{\rm part}$ for different collision energies. To discuss the results of our study in a more summarized way, we then show the different ratios as functions of $\sqrt{s_{NN}}$, for the most central collisions. At first, we show results for both final-state particle distributions and particle distributions at hadronization to see the impact of hadronic cascades on displayed quantities. Finally, we show the proxy and corresponding conserved charge ratios for distributions of all particles at hadronization, compared with the same quantities but only from core particles, in order to highlight the contribution of bulk matter to the fluctuation signal measured in the phase space considered in this analysis.

More detailed results on particle production relevant for the system and collision energies studied in this paper and based on the same set of simulated events can be found in Refs. [31,32].

A. Variances and covariances of identified hadron net multiplicities

In Fig. 5, we show the centrality dependence (via the number of participants, $N_{\rm part}$) of variances of net-π, net-K, net-p, net-Λ, and net-Ξ multiplicities at collision energies $\sqrt{s_{NN}} = 19.6$, 27, 39, 62.4, and 200 GeV. There, one can see variances from final-state particle distributions (full lines) and from particle distributions at hadronization (dashed lines), both from EPOS4, compared with STAR results (dots) [21]. We observe that EPOS4 reproduces qualitatively the expected (quasi-) linear increase with decreasing centrality (increasing $N_{\rm part}$) of the different variances in both distributions. On a quantitative level, EPOS4 results for final-state distributions do not match perfectly the data from STAR, although describing them quite well overall. This is however not of extreme importance in the context of this work, since we only aim at making a quantitative comparative study. Another important aspect to notice in this figure is the difference between variances for particle distribution at hadronization and in the final state. For all hadronic species shown, hadronic cascades increase the variance at all collision energies, by a factor unique to each species which is quite constant regardless of the energy considered. They increase the magnitude of the signal by a factor of approximately two for σ^2_K and σ^2_Ξ to approximately three for σ^2_π and σ^2_p, even up to a factor of approximately four for σ^2_Λ where the effect is the most significant.

In Fig. 6, the same plots are shown for the different covariances $\sigma^{11}_{\pi p}$, $\sigma^{11}_{\pi K}$, and σ^{11}_{pK}. Despite the apparent wiggles observed in the results for covariances, caused by the limited statistics used for this analysis (see Table I), one can conclude similarly to the case of variances that the results from EPOS4 final-state distributions reproduce the qualitative behavior of STAR data and are reasonably close on a quantitative level. We also note an increase of the absolute amplitude of the signal due to hadronic cascades when comparing EPOS4 distributions at hadronization (again shown as a dashed line) with EPOS4 distributions of final-state hadrons (full line).

The observed increase of (co)variances can be explained by the fact that, during hadronic cascades, the numerous inelastic scatterings produce many more of the involved hadronic

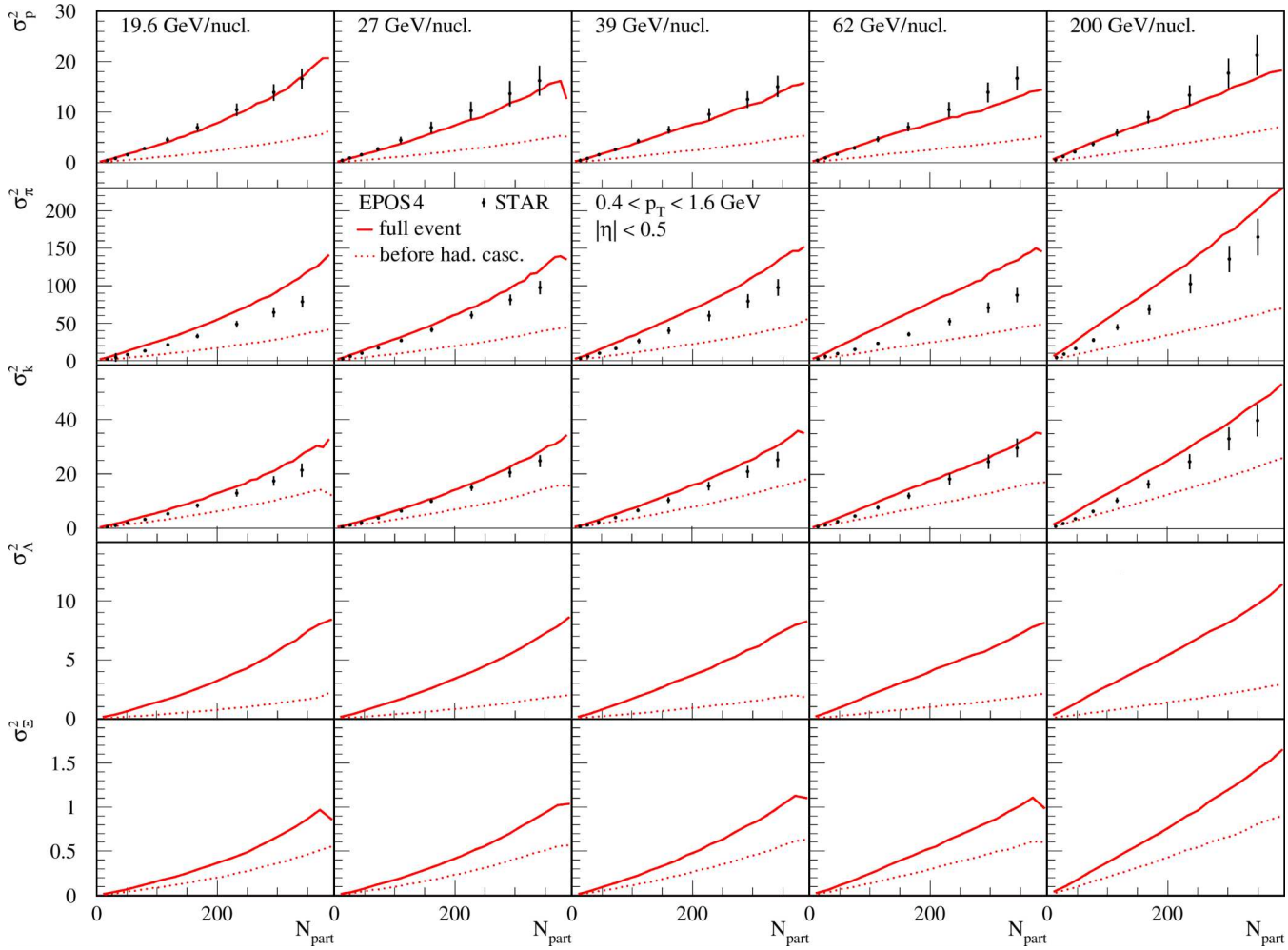

FIG. 5. Net-p, net-π, net-K, net-Λ, and net-Ξ multiplicity variances vs $N_{\rm part}$ for different energies obtained from EPOS4 simulations and compared with STAR available results (dots) [21]. The results calculated from full events are represented by full lines, while results calculated before hadronic cascades are represented by dotted lines.

species, coupled to the successive decays of heavy resonances produced at hadronization. Hence, the successive decays and inelastic scatterings, producing simultaneously several of the hadronic species of interest, lead unavoidably to the amplification of the correlations carried by (co)variances, blurring the actual magnitude of the thermal fluctuations of interest by increasing the signal. These observations support the results of a study led with a hybrid version of UrQMD, which has been coupled to a fluid-dynamical simulation of bulk matter [54]. The authors of Ref. [54] investigated the time-evolution of the correlation of distributions of hadron families carrying conserved charges, compared with the same distributions at hadronization time. The conclusion was that the final distribution of hadrons observed by experiments is not really related anymore to the one obtained after hadronization, which would contain the potential critical signal from the QCD phase transition.

B. Ratios of B, Q, and S cumulants and associated proxies

In Fig. 7, we show the different ratios of second-order conserved charge cumulants with their corresponding proxies, both from EPOS4 and STAR measurements from Ref. [21], as functions of $N_{\rm part}$ for different collision energies. The red curves correspond to the STAR proxy ratios C_{Qp}, C_{QK}, and C_{pK} measured in EPOS4 simulations [defined in Eq. (5)], to be compared with STAR measurements of the same quantities shown as black dots. For each of these three quantities, we also plot in dark blue the corresponding new proposed proxies $\tilde{C}_{QB}$, $\tilde{C}_{QS}$, and $\tilde{C}_{BS} + \tilde{C}'_{BS}$ (in light blue), defined in Eqs. (10), (7), and (8) plus (9), respectively. Finally, we display the corresponding ratios of exact cumulants of conserved charges in green, as a reference. Note that we use this same color code for all figures displaying cumulants ratios.

Let us discuss first the comparison of STAR proxies measured in EPOS4 simulations, with the actual data from Ref. [21] for those quantities. Although variances and covariances computed from EPOS4 simulations do not reproduce perfectly the STAR data, as discussed in the previous section, we notice in Fig. 7 that the proxy ratios C_{Qp}, C_{QK}, and C_{pK} constructed from them do match STAR data point very well on a quantitative level.

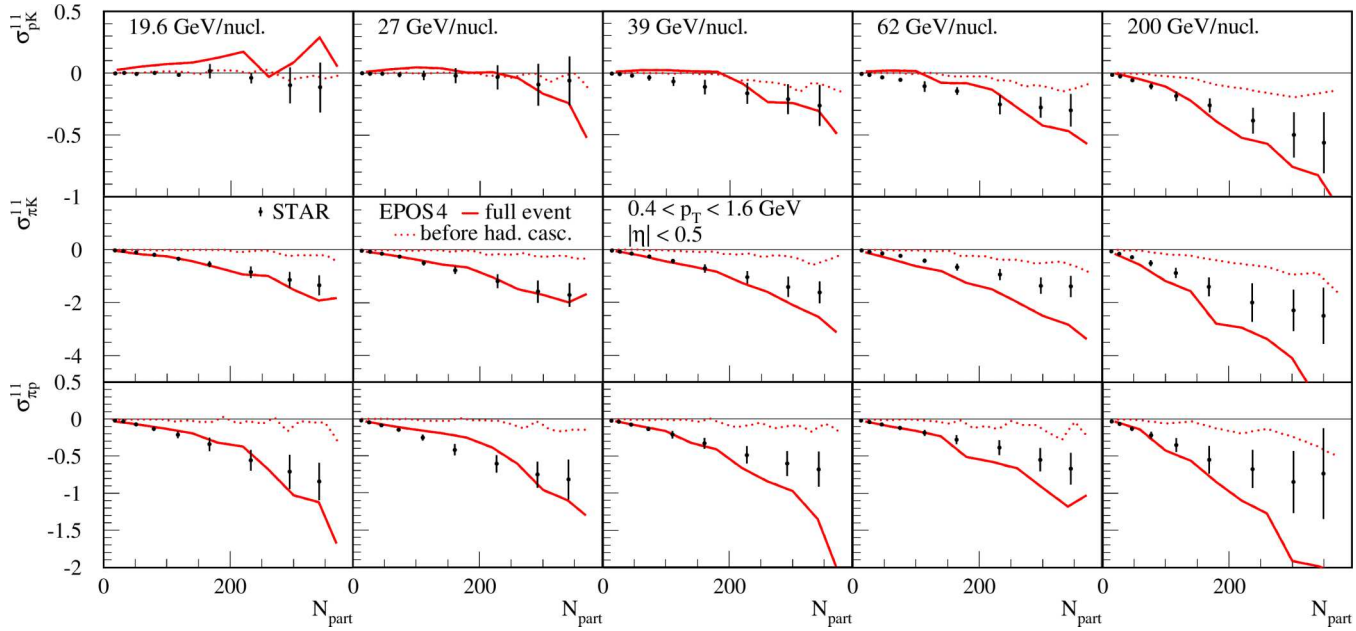

FIG. 6. Covariances of net-p, net-π, and net-K multiplicity distributions vs $N_{\rm part}$ for different energies, obtained from EPOS4 simulations and compared with STAR results (dots) [21]. Results calculated from full events are represented by full lines, while results calculated before hadronic cascades are represented by dotted lines.

Another noticeable feature is the apparent absence of centrality dependence observed for all ratios displayed in Fig. 7 (apart from a slight decrease of the ratio C_{Qp} with increasing $N_{\rm part}$, which appears to be more significant with increasing collision energy). For this reason, we compare from now on the different ratios of conserved charge cumulants with their corresponding proxies as a function of collision energy for central collisions (0%–5% centrality class) only.

Finally, we want to address the case of the ratio $C_{BS} = \sigma^{11}_{BS}/\sigma^2_S$ and its proxies. As an alternative to the STAR proxy C_{pK}, we consider two proxy ratios from Ref. [24], $\tilde{C}_{BS}$ and $\tilde{C}'_{BS}$. While the first one, defined in Eq. (8), relies only on net-Λ variance as a carrier of both strangeness and baryon charge, the second one defined in Eq. (9) also incorporates variances of net-Ξ and net-Ω. However, despite the fact that Ξ and Ω baryons carry respectively a strangeness content of

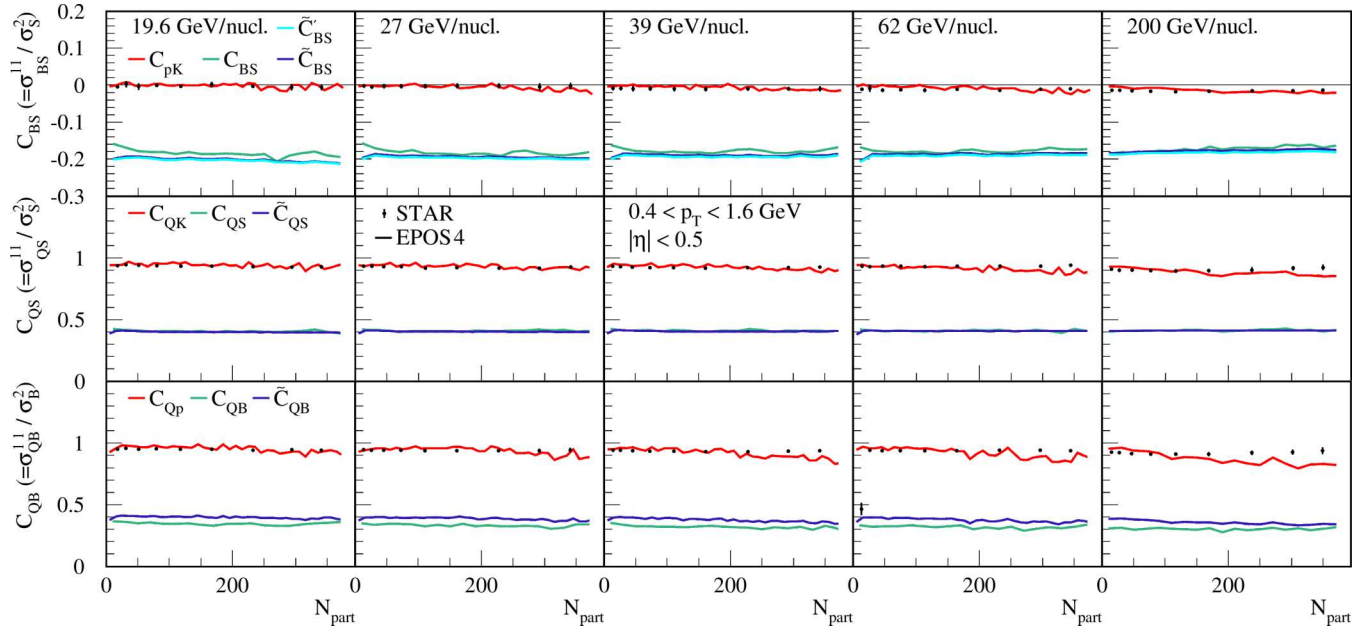

FIG. 7. Ratios of exact B, Q, and S conserved charge (co)variances and their proxies displayed as functions of $N_{\rm part}$ for different energies, obtained from EPOS 3.451 simulations (lines) and compared with STAR data (dots) as a reference [21].

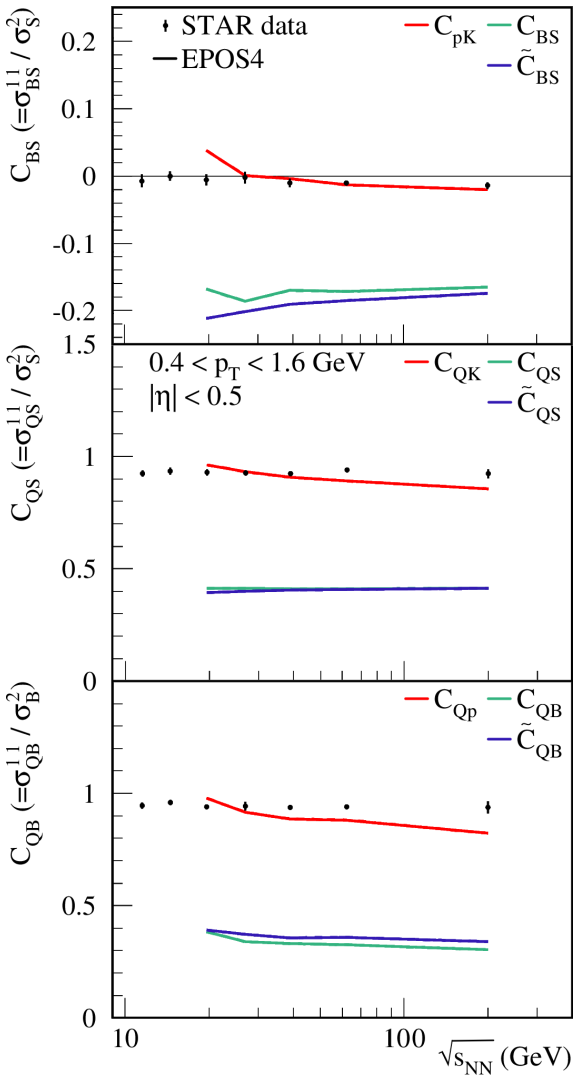

FIG. 8. Ratios of exact B, Q, and S conserved charge (co)variances and their proxies, displayed as functions of $\sqrt{s_{NN}}$ for central collisions (0%–5% centrality class). Results from EPOS4 simulations for final-state particle distributions (lines) are compared with STAR data (dots) as a reference [21].

$|S| = 2$ and $|S| = 3$, they are produced at a significantly lower rate compared with Λ baryons in HICs, approximately one and two orders magnitude less, respectively. This low relative abundance makes their contribution to the C_{BS} proxy ratio almost insignificant in comparison with the net-Λ variance. Looking at the top panels of Fig. 7 showing C_{BS} and related proxies, one can see that $\tilde{C}_{BS}$ and $\tilde{C}'_{BS}$ results completely overlap with each other over the whole centrality range, and for all collision energies displayed. Thus, we choose to discard $\tilde{C}'_{BS}$ from the results from now on and only focus on $\tilde{C}_{BS}$ as a new alternative proxy ratio to C_{BS}. Note that $\tilde{C}_{BS}$ and $\tilde{C}'_{BS}$ have been multiplied by a factor of -1 to match the sign of C_{BS} and σ^2_{pK}, as explicitly defined in Eq. (9).

Coming now to the first main results of our study, we show in Fig. 8 the ratios C_{BS}, C_{QS}, and C_{QB} compared with their respective proxy ratios and STAR results as functions of collision energy $\sqrt{s_{NN}}$ for 0%–5% centrality class events. We observe that the STAR proxy ratios from Eq. (5) measured in EPOS4 simulations are very close to the STAR data (as already noticed previously), despite a slight energy dependence not present in the data. Overall, we note that none of the displayed ratios shows any clear collision energy dependence, for the range that is shown here. However, the important result in these plots lies in the comparison between the ratios of conserved charge cumulants (in green), taken as a reference, and their proxies. STAR data are only shown as a benchmark to see how well EPOS4 can reproduce experimental results. One can observe how remarkably well the new proposed proxies $\tilde{C}_{XY}$ (in blue) are able to reproduce quantitatively the conserved charge cumulant ratios, compared with the STAR proxies C_{QpK} (in red) which show a clear deviation in magnitude. These new proxies are thus shown to be better quantitative probes than those traditionally used by STAR, as well as other experiments to probe fluctuations through second-order cumulants of conserved charges in HICs (see Ref. [55] for a review of these measurements).

C. Impact of hadronic cascades

In Fig. 9, we show all the different ratios and their corresponding proxies as functions of collision energy for the most central collisions (0%–5%), for final-state particle distributions like in Fig. 8 (full lines), but this time compared with their associated value measured at hadronization (dashed lines). As explained in Sec. III, the latter can be measured thanks to the modular construction of EPOS4, which allows us to access particle distributions just after hadronization of the core, before re-interactions between formed hadrons are simulated (using UrQMD in cascade mode).

One can see that the magnitude of almost all ratios is affected very little by the evolution of the system during hadronic cascades, as results for particle distributions at hadronization are very close to their associated value for finale-state distributions. While this result was expected in the case of ratios of conserved charge cumulants, it demonstrates that most proxies discussed here are somehow stable quantities, in the sense that they conserve their magnitude even after the system has gone through hadronic re-interactions which modify its chemistry. Although we have shown in Sec. V A that the (co)variances used to build the proxy ratios are largely impacted by this phase in the evolution of the system, it appears that the modifications of both their respective numerator and denominator compensate overall to leave most of these ratios almost unaffected.

There is one exception to this picture for the proxy ratio $\tilde{C}_{BS}$, which gets a significant modification through hadronic re-interactions. Following the same logic as in the previous paragraph, we understand this to be due to the fact that $\tilde{C}_{BS}$ is built upon σ^2_Λ and σ^2_K, which are the variances that are affected respectively the most and the least from hadronic cascades. In particular, looking at how $\tilde{C}_{BS}$ is constructed in Eq. (8), we see that the numerator consist of σ^2_Λ alone, which gets a growth of about $\approx$4 through the hadronic cascades, while σ^2_K in the denominator is only increased by a factor $\approx$2. Even though the latter is added to σ^2_Λ, their relative difference in magnitude makes σ^2_K dominate the denominator, hence explaining the

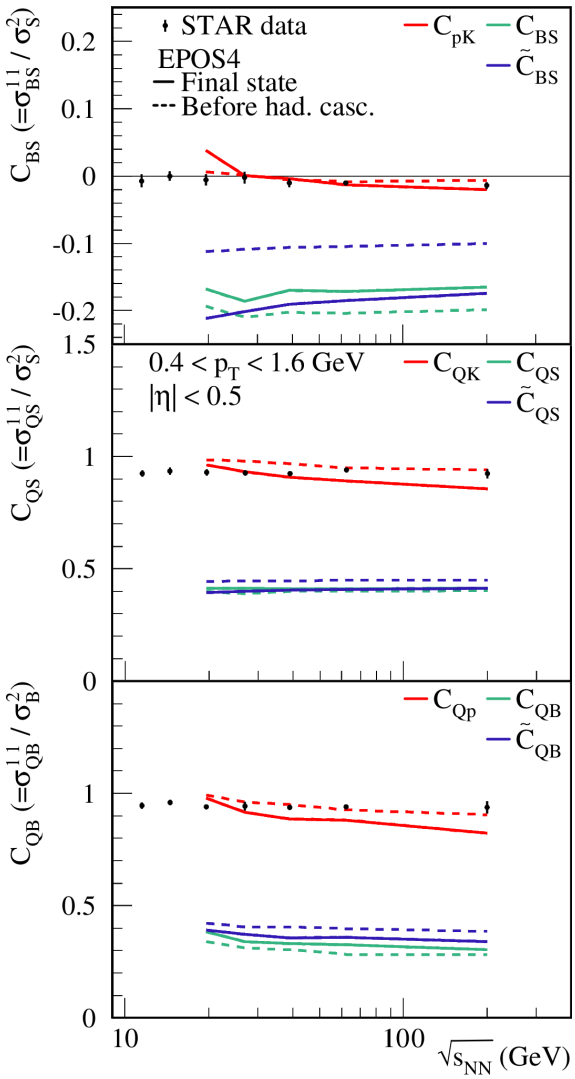

FIG. 9. Ratios of exact B, Q, and S conserved charge (co)variances and their proxies plotted as functions of $\sqrt{s_{NN}}$ for central collisions (0%–5% centrality class). Results are displayed from particle distribution in the final-state (full lines) and before hadronic cascades (dashed lines), from EPOS4 simulations. STAR data (dots) are shown as a reference [21].

increase of $\tilde{C}_{BS}$ after hadronic rescatterings. Such an important growth of net-Λ variance, relative to other hadronic species, might come from the fact that Λ baryons receive an important feed-down contribution from resonance decays, which are not included when considering particles at hadronization time, while they are taken into account when looking at particle distributions in the final state. Moreover, Λ baryons are also less affected by baryon annihilation than protons, as discussed in Ref. [56], which leads to a smaller decrease of σ^2_Λ from this process as compared with σ^2_p, since their net multiplicity will decrease less.

To investigate this issue further, we tried to find another proxy ratio for C_{BS} which would be less modified than $\tilde{C}_{BS}$. Thus, we have computed the following ratio:

$$\tilde{C}^*_{BS} = \frac{\sigma^2_\Xi}{\sigma^2_K + 4\sigma^2_\Xi}, \tag{11}$$

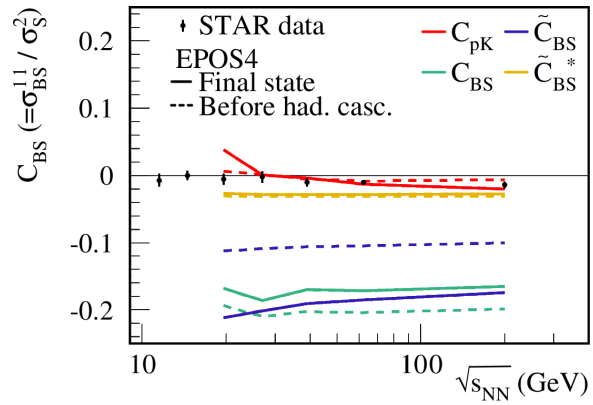

FIG. 10. C_{BS} ratio and different corresponding proxies plotted as functions of $\sqrt{s_{NN}}$ for central collisions (0%–5% centrality class). Results are displayed for full event calculations (full lines) and calculations before hadronic cascades (dashed lines) from EPOS4 simulations. STAR data (dots) are shown as a reference [21].

replacing variance of net-Λ by variance of net-Ξ which, even though produced less abundantly in the system, carries more strangeness and is less impacted by hadronic cascades, as can be seen from Fig. 5. This quantity is compared with C_{BS}, $\tilde{C}_{BS}$, and C_{pK} in Fig. 10, shown in solid yellow for final-state particle distributions and in dashed yellow for distributions before hadronic cascades. We see that although $\tilde{C}^*_{BS}$ suffers almost no change from the hadronic re-interactions phase, it shows a large discrepancy in magnitude with C_{BS}, because the Ξ baryons carry too small a fraction of baryon-strangeness correlation in the system. For this reason, $\tilde{C}_{BS}$ remains the best proxy, especially since it matches C_{BS} very well qualitatively in the final state, which is the only quantity accessible in experiments.

D. Effective contribution from bulk matter

Finally, we show in Fig. 11 the different ratios from particles at hadronization time (dashed lines), compared with the same quantities computed exclusively from particles originating from the core (dotted lines), i.e., the part of the system mimicking the behavior of the QGP. Like in the previous figures, they are displayed as functions of the collision energy for the most central collisions (0%–5%).

We observe that, for every ratio, in both central and peripheral centrality classes, the ratios computed only from core particles at hadronization are overlapping almost perfectly with the ratios computed from all particles at hadronization. This means that the signal measured by the ratios of second-order cumulants in the phase space considered here ($|\eta| < 0.5$ and $0.4 < p_T < 1.6$ GeV) is almost exclusively originating from the bulk matter, modeled by the core in EPOS4. Hence, if the system created in such collisions would endure critical behavior, these ratios should indeed be sensitive to it and carry its signature as long as they are measured in a similar phase space.

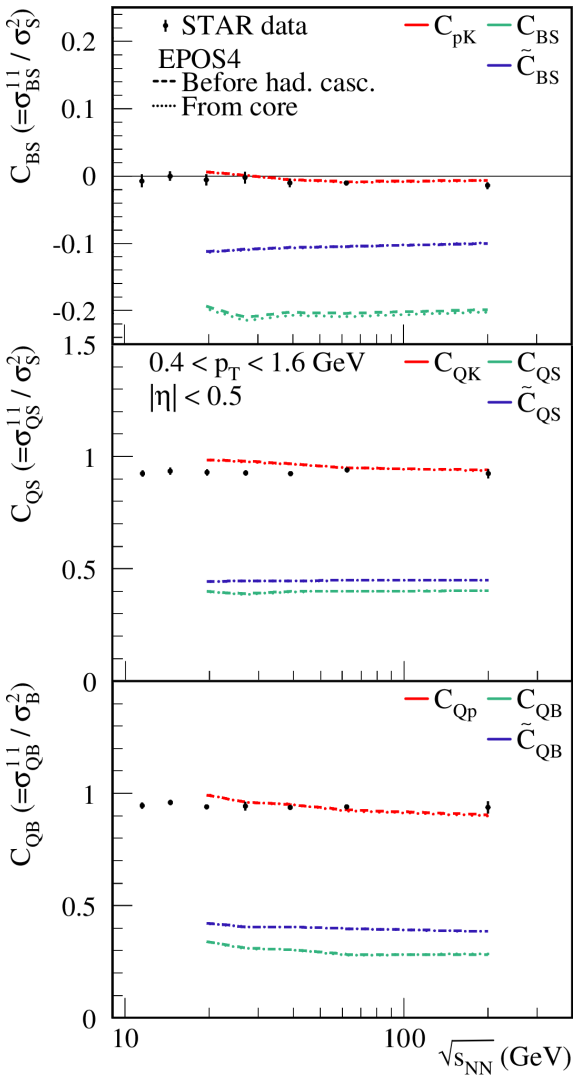

FIG. 11. Core proportion of C_{XY} and enhanced proxies $\tilde{C}_{XY}$ ratios over the total value calculated before hadronic cascades, plotted as a function of $\sqrt{s_{NN}}$ for central collisions (0%–5% centrality class). Ratios of exact B, Q, and S conserved charge (co)variances and their proxies plotted as functions of $\sqrt{s_{NN}}$ for central collisions (0%–5% centrality class). Results are displayed from particle distribution before hadronic cascades (dashed lines) and from core particles only (dotted lines), from EPOS4 simulations. STAR data (dots) are shown as a reference [21].

VI. SUMMARY AND OUTLOOKS

We discussed the use of new proxies for conserved charge cumulants, which are of primary importance in the study of correlations between conserved charges B, Q, and S and expected to be key observables in the search for the existence of a critical point in the phase diagram of nuclear matter. The new quantities $\tilde{C}_{QS}$ and $\tilde{C}_{BS}$, proposed in Ref. [24], as well as $\tilde{C}_{QB}$ which we proposed based on that previous study, are compared with corresponding proxies commonly measured in experiment, C_{QK}, C_{pK}, and C_{Qp}, as well as their counterparts based on exact conserved charge quantities. We employed EPOS4 to evaluate all these observables through simulations of Au + Au collisions at energies $\sqrt{s_{NN}} = 19.6$–200 GeV, where data were also available for comparison in Ref. [21], in order to assess the actual performance of the new proxies in the context of a realistic out-of-equilibrium system close to the one created experimentally.

The results of our study showed that the proposed proxies are better at reproducing their corresponding conserved charge cumulant ratios, as compared with the equivalent STAR proxies. We note first of all that, with the only exception of $\tilde{C}_{BQ}$, all these quantities are uniquely built upon variances. This makes sense, since correlations between different conserved charges are naturally carried by some hadron species (e.g., B and Q by the protons, Q and S by kaons, or B and S by Λ baryons). Moreover, we observe that the addition of σ^2_Λ alone to the already measured σ^2_π, σ^2_K, and σ^2_p is enough to build those new proxies. Luckily, this quantity was already measured (although in a different phase space) by STAR and published in Ref. [37].

We compared the different ratios measured from final-state particle distributions to their value measured from particle distribution at hadronization time. This way, we were able to quantify the effect of hadronic cascades on these quantities. While the ratio of conserved charge cumulants are almost not affected by hadronic rescatterings, as expected, we can also see that $\tilde{C}_{QB}$ and $\tilde{C}_{QS}$ are also left unchanged after the hadronic cascades. For this reason, they represent excellent proxies of their corresponding ratios of conserved charge cumulants C_{QB} and C_{QS}. The only significant deviation between measurement at hadronization and in the final state is observed for $\tilde{C}_{BS}$. We saw that this discrepancy originates from the fact that σ^2_Λ is more enhanced by hadronic cascades than other net-variances, in particular σ^2_K. Potential reasons to explain this difference have been discussed.

Finally, we investigated how much of the signal, for the phase space used in this analysis, is actually coming from particles originating from the bulk matter of the system. Unsurprisingly, the quasi totality of the signal effectively originates from the core in EPOS4, meaning that measuring net cumulants of hadronic species within $|\eta| < 0.5$ and with $0.4 < p_T < 1.6$ GeV actually probes fluctuations coming uniquely from bulk matter. Hence, if the system created in such collisions was to experience the impact of a critical point during its evolution, fluctuation observables should carry its imprint.

It would be interesting to test the ability of the new proxy ratios $\tilde{C}_{QB}$, $\tilde{C}_{QS}$, and $\tilde{C}_{BS}$ to reproduce their corresponding ratios of cumulants of conserved charges at lower collision energies, compared with those shown in this work. Most of the studies published in recent years seem to point at a collision-energy range $\sqrt{s_{NN}} \approx 1$–20 GeV to observe phenomena which could hint at the existence of a critical point [13]. Hence, using transport models which are suited for modeling the dynamics of HICs at these energies seems highly relevant and timely; see Ref. [57] for a recent review of the status of such models.

Investigating with more details the impact of the hadronic rescatterings on the new proxy ratios, in particular within the previously mentioned collision-energy range, is also important to ensure their robustness through the evolution of the

system. Some work in this direction has already been initiated, for instance by using an extended particle list to study the impact of resonances in Ref. [58], or by including mean-field potentials to model hadron interactions in a more realistic manner in transport approaches [59].

ACKNOWLEDGMENTS

J.J. thanks Jean-Yves Ollitrault, Marlene Nahrgang, and Grégoire Pihan for the instructive discussions about this work, as well as Volodymyr Vovchenko for the careful read and constructive feedback on this paper. This material is based upon work supported by the National Science Foundation under Grants No. PHY-2208724, No. PHY-1654219, and No. PHY-2116686, and within the framework of the MUSES Collaboration, under Grant No. OAC- 2103680. This material is also based upon work supported by the U.S. Department of Energy, Office of Science, Office of Nuclear Physics, under Award No. DE-SC0022023 and Grant No. DE-SC0020651.

[1] I. Arsene *et al.* (BRAHMS Collaboration), Quark gluon plasma and color glass condensate at RHIC? The perspective from the BRAHMS experiment, Nucl. Phys. A **757**, 1 (2005).
[2] B. B. Back *et al.* (PHOBOS Collaboration), The PHOBOS perspective on discoveries at RHIC, Nucl. Phys. A **757**, 28 (2005).
[3] J. Adams *et al.* (STAR Collaboration), Experimental and theoretical challenges in the search for the quark gluon plasma: The STAR Collaboration's critical assessment of the evidence from RHIC collisions, Nucl. Phys. A **757**, 102 (2005).
[4] K. Adcox *et al.* (PHENIX Collaboration), Formation of dense partonic matter in relativistic nucleus-nucleus collisions at RHIC: Experimental evaluation by the PHENIX collaboration, Nucl. Phys. A **757**, 184 (2005).
[5] Y. Aoki, G. Endrodi, Z. Fodor, S. D. Katz, and K. K. Szabó, The Order of the quantum chromodynamics transition predicted by the standard model of particle physics, Nature (London) **443**, 675 (2006).
[6] A. Bazavov *et al.* (HotQCD), Chiral crossover in QCD at zero and non-zero chemical potentials, Phys. Lett. B **795**, 15 (2019).
[7] S. Borsanyi, Z. Fodor, J. N. Guenther, R. Kara, S. D. Katz, P. Parotto, A. Pasztor, C. Ratti, and K. K. Szabó, QCD crossover at finite chemical potential from lattice simulations, Phys. Rev. Lett. **125**, 052001 (2020).
[8] T. Niida and Y. Miake, Signatures of QGP at RHIC and the LHC, AAPPS Bull. **31**, 12 (2021).
[9] C. S. Fischer, QCD at finite temperature and chemical potential from Dyson–Schwinger equations, Prog. Part. Nucl. Phys. **105**, 1 (2019).
[10] D. Fuseau, T. Steinert, and J. Aichelin, Phase diagram of the Polyakov–Nambu–Jona-Lasinio approach for finite chemical potentials, Phys. Rev. C **101**, 065203 (2020).
[11] W.-J. Fu, J. M. Pawlowski, and F. Rennecke, QCD phase structure at finite temperature and density, Phys. Rev. D **101**, 054032 (2020).
[12] M. Hippert, J. Grefa, T. A. Manning, J. Noronha, J. Noronha-Hostler, I. Portillo Vazquez, C. Ratti, R. Rougemont, and M. Trujillo, Bayesian location of the QCD critical point from a holographic perspective, arXiv:2309.00579.
[13] A. Bzdak, S. Esumi, V. Koch, J. Liao, M. Stephanov, and N. Xu, Mapping the phases of quantum chromodynamics with beam energy scan, Phys. Rep. **853**, 1 (2020).
[14] D. Tlusty, The RHIC beam energy scan phase II: Physics and upgrades, arXiv:1810.04767.
[15] K. C. Meehan (STAR Collaboration), Fixed target collisions at STAR, Nucl. Phys. A **956**, 878 (2016).
[16] R. Bellwied, S. Borsanyi, Z. Fodor, S. D. Katz, A. Pásztor, C. Ratti, and K. K. Szabó, Fluctuations and correlations in high temperature QCD, Phys. Rev. D **92**, 114505 (2015).
[17] X. Luo and N. Xu, Search for the QCD critical point with fluctuations of conserved quantities in relativistic heavy-ion collisions at RHIC: an overview, Nucl. Sci. Tech. **28**, 112 (2017).
[18] M. A. Stephanov, Non-Gaussian fluctuations near the QCD critical point, Phys. Rev. Lett. **102**, 032301 (2009).
[19] M. Abdallah *et al.* (STAR Collaboration), Cumulants and correlation functions of net-proton, proton, and antiproton multiplicity distributions in Au + Au collisions at energies available at the BNL relativistic heavy ion collider, Phys. Rev. C **104**, 024902 (2021).
[20] L. Adamczyk *et al.* (STAR Collaboration), Collision energy dependence of moments of net-kaon multiplicity distributions at RHIC, Phys. Lett. B **785**, 551 (2018).
[21] J. Adam *et al.* (STAR Collaboration), Collision-energy dependence of second-order off-diagonal and diagonal cumulants of net-charge, net-proton, and net-kaon multiplicity distributions in Au + Au collisions, Phys. Rev. C **100**, 014902 (2019); **105**, 029901(E) (2022).
[22] M. Bluhm, A. Kalweit, M. Nahrgang, M. Arslandok, P. Braun-Munzinger, S. Floerchinger, E. S. Fraga, M. Gazdzicki, C. Hartnack, C. Herold *et al.*, Dynamics of critical fluctuations: Theory – phenomenology – heavy-ion collisions, Nucl. Phys. A **1003**, 122016 (2020).
[23] V. Koch, A. Majumder, and J. Randrup, Baryon-strangeness correlations: A diagnostic of strongly interacting matter, Phys. Rev. Lett. **95**, 182301 (2005).
[24] R. Bellwied, S. Borsanyi, Z. Fodor, J. N. Guenther, J. Noronha-Hostler, P. Parotto, A. Pásztor, C. Ratti, and J. M. Stafford, Off-diagonal correlators of conserved charges from lattice QCD and how to relate them to experiment, Phys. Rev. D **101**, 034506 (2020).
[25] K. Werner, Revealing a deep connection between factorization and saturation: New insight into modeling high-energy proton-proton and nucleus-nucleus scattering in the EPOS4 framework, Phys. Rev. C **108**, 064903 (2023).
[26] N. R. Sahoo, S. De, and T. K. Nayak, Baseline study for higher moments of net-charge distributions at energies available at the BNL relativistic heavy ion collider, Phys. Rev. C **87**, 044906 (2013).
[27] V. Vovchenko and V. Koch, Efficiency corrections for factorial moments and cumulants of overlapping sets of particles, Nucl. Phys. A **1010**, 122179 (2021).

[28] A. Chatterjee, T. Nonaka, S. Esumi, and X. Luo, Efficiency corrections for mutually inclusive variables and particle identification effect for mixed-cumulants in heavy-ion collisions, Chin. Phys. C **45**, 104001 (2021).

[29] P. Alba, R. Bellwied, S. Borsányi, Z. Fodor, J. Günther, S. D. Katz, V. M. Sarti, J. Noronha-Hostler, P. Parotto, A. Pasztor *et al.*, Constraining the hadronic spectrum through QCD thermodynamics on the lattice, Phys. Rev. D **96**, 034517 (2017).

[30] M. S. Abdallah *et al.* (STAR Collaboration), Disappearance of partonic collectivity in $\sqrt{s_{NN}} = 3$ GeV Au + Au collisions at RHIC, Phys. Lett. B **827**, 137003 (2022).

[31] K. Werner, J. Jahan, I. Karpenko, T. Pierog, M. Stefaniak, and D. Vintache, Heavy ion collisions from $\sqrt{s_{NN}}$ of 62.4 GeV down to 4 GeV in the EPOS4 framework, arXiv:2401.11275.

[32] K. Werner, Parallel scattering, saturation, and generalized Abramovskii-Gribov-Kancheli (AGK) theorem in the EPOS4 framework, with applications for heavy-ion collisions at $\sqrt{s_{NN}}$ of 5.02 TeV and 200 GeV, Phys. Rev. C **109**, 034918 (2024).

[33] M. Bluhm and M. Nahrgang, Freeze-out conditions from strangeness observables at RHIC, Eur. Phys. J. C **79**, 155 (2019).

[34] V. Vovchenko and H. Stoecker, Thermal-FIST: A package for heavy-ion collisions and hadronic equation of state, Comput. Phys. Commun. **244**, 295 (2019).

[35] M. Kitazawa and M. Asakawa, Revealing baryon number fluctuations from proton number fluctuations in relativistic heavy ion collisions, Phys. Rev. C **85**, 021901(R) (2012).

[36] M. Kitazawa and M. Asakawa, Relation between baryon number fluctuations and experimentally observed proton number fluctuations in relativistic heavy ion collisions, Phys. Rev. C **86**, 024904 (2012); **86**, 069902(E) (2012).

[37] J. Adam *et al.* (STAR Collaboration), Beam energy dependence of net-Λ fluctuations measured by the STAR experiment at the BNL relativistic heavy ion collider, Phys. Rev. C **102**, 024903 (2020).

[38] J. M. Campbell, M. Diefenthaler, T. J. Hobbs, S. Höche, J. Isaacson, F. Kling, S. Mrenna, J. Reuter, S. Alioli, J. R. Andersen *et al.*, Event generators for high-energy physics experiments, SciPost Phys. **16**, 130 (2022).

[39] https://klaus.pages.in2p3.fr/epos4/.

[40] H. J. Drescher, M. Hladik, S. Ostapchenko, T. Pierog, and K. Werner, Parton based Gribov-Regge theory, Phys. Rep. **350**, 93 (2001).

[41] K. Werner and B. Guiot, Perturbative QCD concerning light and heavy flavor in the EPOS4 framework, Phys. Rev. C **108**, 034904 (2023).

[42] K. Werner, Core-corona separation in ultra-relativistic heavy ion collisions, Phys. Rev. Lett. **98**, 152301 (2007).

[43] K. Werner, B. Guiot, I. Karpenko, and T. Pierog, Analysing radial flow features in *p*-Pb and *p*-*p* collisions at several TeV by studying identified particle production in EPOS3, Phys. Rev. C **89**, 064903 (2014).

[44] K. Werner, Core-corona procedure and microcanonical hadronization to understand strangeness enhancement in proton-proton and heavy ion collisions in the EPOS4 framework, Phys. Rev. C **109**, 014910 (2024).

[45] I. Karpenko, P. Huovinen, and M. Bleicher, A 3 + 1 dimensional viscous hydrodynamic code for relativistic heavy ion collisions, Comput. Phys. Commun. **185**, 3016 (2014).

[46] M. Bleicher, E. Zabrodin, C. Spieles, S. A. Bass, C. Ernst, S. Soff, L. Bravina, M. Belkacem, H. Weber, H. Stöcker *et al.*, Relativistic hadron hadron collisions in the ultrarelativistic quantum molecular dynamics model, J. Phys. G **25**, 1859 (1999).

[47] H. Petersen, J. Steinheimer, G. Burau, M. Bleicher, and H. Stöcker, A fully integrated transport approach to heavy ion reactions with an intermediate hydrodynamic stage, Phys. Rev. C **78**, 044901 (2008).

[48] P. Parotto, M. Bluhm, D. Mroczek, M. Nahrgang, J. Noronha-Hostler, K. Rajagopal, C. Ratti, T. Schäfer, and M. Stephanov, QCD equation of state matched to lattice data and exhibiting a critical point singularity, Phys. Rev. C **101**, 034901 (2020).

[49] M. Kahangirwe, S. A. Bass, E. Bratkovskaya, J. Jahan, P. Moreau, P. Parotto, D. Price, C. Ratti, O. Soloveva, and M. Stephanov, Finite density QCD equation of state: Critical point and lattice-based T' expansion, Phys. Rev. D **109**, 094046 (2024).

[50] M. Stefaniak, K. Werner, H. P. Zbroszczyk, and J. Jahan, Equation of state within the EPOS3 model, Phys. Rev. C **108**, 014905 (2023).

[51] M. Stephanov and Y. Yin, Hydrodynamics with parametric slowing down and fluctuations near the critical point, Phys. Rev. D **98**, 036006 (2018).

[52] G. Pihan, M. Bluhm, M. Kitazawa, T. Sami, and M. Nahrgang, Critical net-baryon fluctuations in an expanding system, Phys. Rev. C **107**, 014908 (2023).

[53] J. Jahan, The beam energy scan under the scope of EPOS 4, Ph.D. thesis, Nantes Université, 2022.

[54] J. Steinheimer, V. Vovchenko, J. Aichelin, M. Bleicher, and H. Stöcker, Conserved charge fluctuations are not conserved during the hadronic phase, Phys. Lett. B **776**, 32 (2018).

[55] R. Kumar *et al.* (MUSES Collaboration), Theoretical and experimental constraints for the equation of state of dense and hot matter, Living Rev. Relativ. **27**, 3 (2024).

[56] J. Steinheimer, J. Aichelin, M. Bleicher, and H. Stöcker, Influence of the hadronic phase on observables in ultrarelativistic heavy ion collisions, Phys. Rev. C **95**, 064902 (2017).

[57] H. Wolter *et al.* (TMEP Collaboration), Transport model comparison studies of intermediate-energy heavy-ion collisions, Prog. Part. Nucl. Phys. **125**, 103962 (2022).

[58] J. Hammelmann, M. Bluhm, M. Nahrang, and H. Elfner, Fate of critical fluctuations in an interacting hadronic medium using maximum entropy distributions, arXiv:2310.06636.

[59] A. Sorensen and V. Koch, Phase transitions and critical behavior in hadronic transport with a relativistic density functional equation of state, Phys. Rev. C **104**, 034904 (2021).